

Searching for Mass Concentrations with Precision Pulsar Timing

JOHN M. LoSECCO¹

¹*Physics and Astronomy Department, University of Notre Dame, Notre Dame, IN 46556-5670, USA*

ABSTRACT

This paper searches for evidence of mass concentrations along the path of radio pulses in the PPTA2 survey data release. Radio pulse travel times are influenced via gravitational fields along the path from the source to the observer. Transient time delays in transit are a useful measure of the matter distribution along the path. Many pulsars have very well understood timing solutions with predictable arrival times and can be used to sample the mass variation. Changes in the source, observer and mass concentration positions produce changes in arrival times which can be significant for precision pulsar times. Twelve candidates are reported from this search.

Keywords: dark matter pulsars: general proper motions time gravitation

1. INTRODUCTION

Gravitational interactions have been suggested as a source of transient distortions in pulsar arrival time. Larchenkova (1995). Recently efforts have been made to understand and correct for a broad class of timing distortions in pulsar arrival times with results approaching microsecond resolution. This suggests that searching these data may help strengthen models of galactic mass distributions.

In this note we search for the relativistic delay in pulsar pulses due to encounters with the gravitational fields of masses distributed close the path of source to observer, as illustrated in figure 1. A static mass distribution would add an unmeasurable constant time delay to the signal, so just as in other mass concentration searches Wyrzykowski (2022) one looks for a time delay caused by a transient encounter.

The accumulated time delay is given by Shapiro (1964); Larchenkova (2007):

$$\Delta T = -\frac{2GM}{c^3} \ln(1 - \hat{R} \cdot \hat{s}) \quad (1)$$

where $\frac{2GM}{c^3}$ is the Schwarzschild radius divided by the speed of light and $\hat{R} \cdot \hat{s}$ is the cosine of the angle, as viewed from the observer, between the source of the pulse and the source of the gravitational field created by mass \mathcal{M} .

Pulsar timing arrays Kerr (2021) have improved arrival time fits for pulses and modeled the various known sources of time deviations in the transit time. Orbital motion of the source and the observer can be fit and removed. Observing

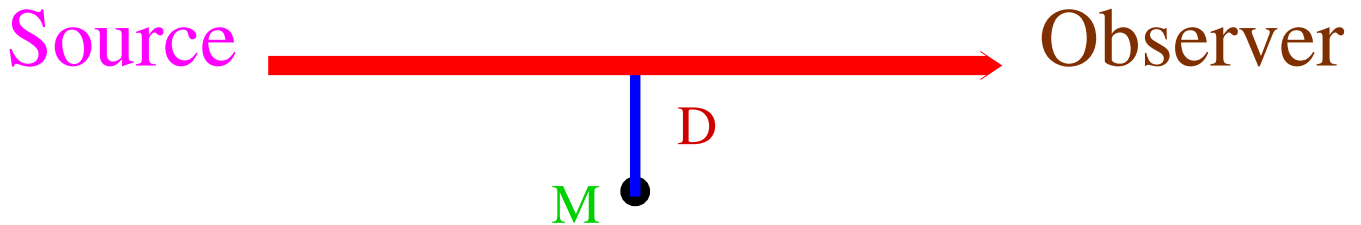


Figure 1. An illustration of the source to observer geometry. The impact parameter D and the gravitating mass \mathcal{M} are shown.

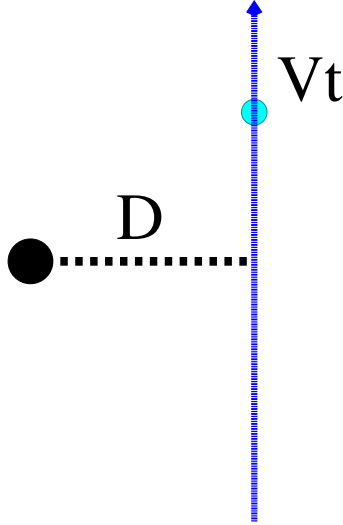


Figure 2. The time dependent geometry of the pulsar - mass concentration cosine as viewed by the observer. The Z axis goes from the observer to the pulsar (dot on the left). The point of closest approach is a distance D along the X axis. The Y coordinate is upward along the projected speed of the mass concentration. The displacement along Y is taken as Vt . The mass concentration is in the plane at (D, Vt) .

at multiple frequencies permits removal of frequency dependent plasma delays. Even the relativistic delay caused by a massive companion of the pulsar can be fit and removed.

2. GRAVITATIONAL TIME DELAY

In this paper we fit the pulsar timing residuals of the PPTA2 survey sources [Kerr \(2021\)](#) to a 4 parameter model of an encounter of the beam with a mass source moving with constant speed in the plane of the observation.

[Larchenkova \(1995\)](#) suggest the 4 parameter fit of equation 2.

$$\Delta T = -M \ln \left(1 - \frac{1}{\sqrt{1 + (v(t - t_0))^2 + d^2}} \right) \quad (2)$$

with $M = \frac{2GM}{c^3}$ as the mass of the source of the field (in units of microseconds), t_0 is the time of the closest encounter, v is the (assumed) constant projected speed of the encounter and d is the distance of closest approach, at $t = t_0$. For reference M_{sun} is 9.85 microseconds. To be more precise d is the tangent of the angle of closest approach and $v(t - t_0)$ is the tangent of the angle from the point of closest approach to the location at time t

Equation 2 is found by explicitly calculating the value of $\hat{R} \cdot \hat{s}$ in the geometry shown in figure 2. Take the \hat{z} axis along the direction from the observer to the pulsar. The distance from the pulsar beam path to the mass concentration candidate point of closest approach is D . The direction from the pulsar beam path to the mass concentration candidate point of closest approach defines the \hat{x} axis. The vertical axis in the figure is the \hat{y} axis and is the direction of motion of the mass concentration candidate. The Z distance is arbitrary but we can take it as the distance along the \hat{z} axis to the point of closest approach of the beam to the mass concentration candidate. Figure 2 is drawn in the plane perpendicular to the \hat{z} axis at distance Z. In this coordinate system $\vec{R} = (0, 0, Z)$ and $\vec{s} = (D, Vt, Z)$.

$$\begin{aligned} \hat{R} \cdot \hat{s} &= \frac{Z^2}{Z \times \sqrt{Z^2 + (Vt)^2 + D^2}} \\ &= \frac{Z^2}{Z^2 \sqrt{1 + (vt)^2 + d^2}} \\ &= \frac{1}{\sqrt{1 + (vt)^2 + d^2}} \end{aligned} \quad (3)$$

which is equation 2 with $d = D/Z$ and $v = V/Z$.

3. THE DATA

The PPTA2 release [Antoniadis \(2022\)](#) includes 65 millisecond pulsars and their fits. This data was processed with *Tempo2* [Edwards \(2006\)](#) to provide residuals, the deviation of the pulse arrival time from the time estimated by the model. These residuals hold information about potential encounters with massive bodies on route to the detector.

The IPTA data release 2 combines data from prior releases, EPTA 1, NANOGrav 9-year, PPTA and their extensions. The observations have been made by seven different radio telescopes (Effelsberg, Lovell, Nançay, Westerbork, Green Bank, Arecibo, Parkes) The pulsar data samples span varying time intervals from 231 to 10753 days and have from 116 to 17487 fitted pulses. A total of 210148 pulse residuals over a total time period of 255327 MJD are provided in the release.

4. METHOD

The method used has two parts. The first part searches for signal delay candidates over a limited portion of the recorded data. Once found a local fit is done on that candidate to recover the fit parameters.

Based on gravitational lensing results the encounters are expected to occur over a period of weeks or months. The data sample span periods from less than a year to almost 30 years. Reliable fits also require many more data points to be fit compared to the four parameters to be measured. The method adopted is to fit overlapping regions of at about 120 consecutive residuals, less if there is not enough data to provide 120 samples. A modest event candidate is refit with the candidate time at the center of the interval. When possible the time width of the fit is chosen to be the point where the peak has dropped to 10% of its maximum height. The peak position and width are based on the parameters extracted from the search step. The fit is sensitive to the tails of the fit function so having two tails to fit helps reject noise. If the candidate time is near either end of the data sample that tail is truncated. Using a sample size large compared to the encounter time makes the fit more sensitive to fluctuations in the underlying tempo2 fit since the fit curve returns to zero on both sides of an encounter. An example of a fit is in [figure 3](#)

To proceed from the search fit to the centered fit the search result must have a log likelihood ratio test at the 95% level. The fit itself should have an Anderson-Darling test for gaussian residuals at the 95% level and the absolute value of the fitted mass, $|M|$ must be at least 3 time its σ . Accepting $M < -3\sigma$ is included to study potential background fluctuations indicated by negative time delays with the same time structure expected from a point mass.

The same selection plus the requirement that χ^2/DOF probability is greater than 10% is applied to the centered fit before it can be accepted as a Shapiro delay candidate.

5. TECHNICAL DETAILS

From [equation 1](#) it is clear that the fit can diverge as $\hat{R} \cdot \hat{s} \rightarrow 1$. Since the residual data is finite it is unlikely that the solution will fall on this point but the fitter may still explore this region to approach the best fit. Due to finite precision of computer representations of numbers $1 - \cos \theta$ may approach 0 more rapidly due to loss of precision. The fitter uses the “log1p” function of $-\cos \theta$ to delay the round off error in the logarithm function evaluation. At even smaller values of θ the approximation of $1 - \cos \theta = \theta^2/2$ is used as the argument to the logarithm. Eventually that is replaced with $\ln(\theta^2/2) = 2 \ln(\theta) - \ln(2)$. This provides access to a maximum amplification of about 1490 with standard double precision calculations.

The transition from search to fit uses the preliminary fitted velocity from the search to determine the temporal range of the fit. Ideally one wants a time range in which the fit is dominated by the signal and not the asymptotic tails which should go to zero. The first attempt is to construct a time symmetric region about the candidate time with the amplitude dropping to 10% of the peak height. In the case of a very local fluctuation the search fitted velocity is very large and one ends up with very few timing residuals in the narrow time range. To get more statistics the refit region is expanded to get at least 100 points.

Alternatively a systematic shift in the residuals raises the baseline. There is no baseline parameter in the fit so this is turned into a very small velocity. The small velocity results in a very large time range for the refit, sometimes including the whole data sample for the pulsar. The refitting for nearby search regions then have a large overlap, reducing their independence. In this case the refit is shortened to under 500 residuals.

In both cases the refit sample is centered on the candidate to the extent possible and the initial values for the refit parameters are those taken from the search. “to the extent possible” is needed since the data itself is not uniformly sampled in time and is a merger of data from multiple instruments. The search time is put in the middle of the refit sample. Gaps in the data sample and different sampling rates may cause the centered fit to not have the same number

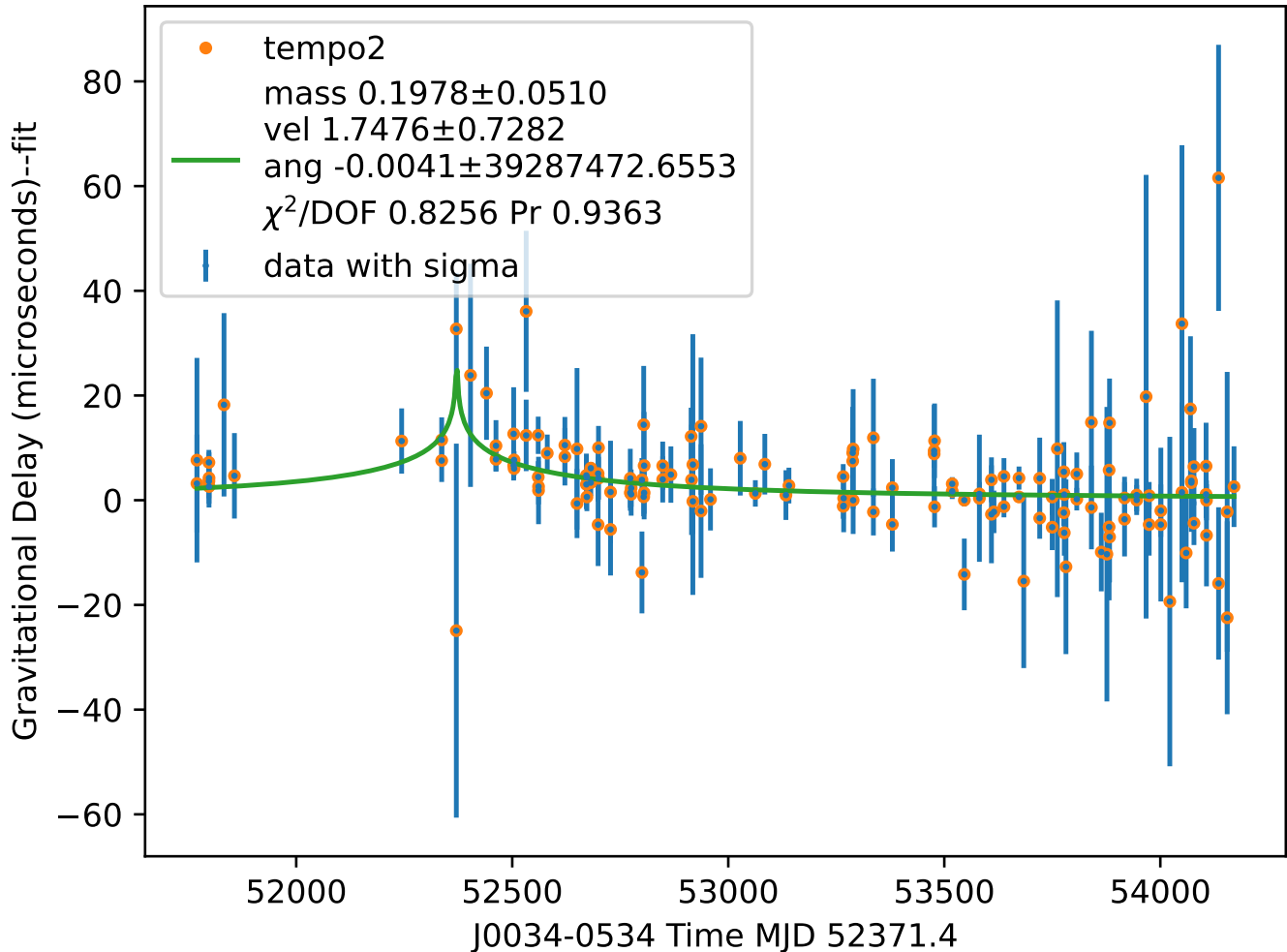


Figure 3. A fit to pulsar J0034-0534 showing a significant delay at 52371.4 MJD.

of residuals before and after the event time. Lower or upper time limits of the whole data sample also restrict the range for the centered fit.

In the case of low velocities this adjustment procedure may produce a small bias against a true signal with the direction of proper motion close to the line of sight. On the other hand the search samples may have a non-zero offset, perhaps coming from very long period signals. A symptom of such an offset is a very small value for v . If $v\Delta t < 10$ mrad the offset is removed by subtracting the sample mean from the sample. Δt is the actual time length of the fit sample. This baseline adjustment was not needed for any of the candidate encounters in this paper.

An MCMC based search was used to explore the parameter space near the solution to improve the error estimates. A fit was accepted as a candidate if $\mathcal{M}/\sigma_{\mathcal{M}} > 3$ and the χ^2/DOF probability exceed 0.1.

6. RESULTS

2084 candidates pass the search criteria to be recentered and refit. After the refit 108 of these have $\mathcal{M}/\sigma_{\mathcal{M}} > 3$. 16 of these have a fit with a χ^2/DOF probability > 0.1 , the criteria in the centered fit to become a final event candidate. Since the search uses overlapping regions and the centered fit can extend the fit into regions already fit there are duplicate candidates in some cases. Since the data samples do not overlap completely the duplicates are not identical but the date is very close and the other parameters agree to fractions of a σ . The 4 duplicates have been removed from the table.

Pulsar	Sample	Duration	Count	RMS	Prob	$\mathcal{M} \pm \sigma_{\mathcal{M}}$	$\mathcal{M}/\sigma_{\mathcal{M}}$
J0613-0200	19	236.8	457	3.551	0.9995	0.01644 ± 0.004938	3.329
J1024-0719	29	111.7	414	10.54	0.9139	-0.4137 ± 0.07403	-5.588
J0034-0534	0	2011.4	109	9.095	0.8481	1.656 ± 0.3839	4.314
J1024-0719	75	94.7	446	7.891	0.6924	0.3192 ± 0.1049	3.042
J1713+0747	211	53.3	452	2.111	0.6369	0.03642 ± 0.009973	3.652
J1640+2224	3	84.1	153	4.339	0.6173	0.06589 ± 0.01322	4.984
J1857+0943	46	127.4	403	2.747	0.4474	0.05748 ± 0.009663	5.948
J1909-3744	175	54.2	476	1.273	0.2458	0.01408 ± 0.003733	3.772
J1643-1224	17	230.7	399	3.563	0.1902	0.4636 ± 0.09352	4.957
J1024-0719	39	123.7	442	10.72	0.1343	-0.2983 ± 0.07129	-4.184
J0613-0200	72	70	436	2.661	0.1122	0.03849 ± 0.01255	3.068
J1643-1224	1	1765.6	103	10.78	0.1056	-2.206 ± 0.4336	-5.087

Table 1. There are 12 candidates after duplicates have been removed. Eight pulsars are represented. The first 4 columns give details of the fit sample including the time duration of the sample and the number of points fit. The fifth column gives the RMS value of the residuals used in the fit as a measure of the noise level in the sample. The last 3 columns give the result of the centered 10% fit including the χ^2 confidence of the fit, the mass fitted and the significance of the mass fit in σ 's. The RMS and the mass are given in microseconds.

Pulsar	Sample	$\mathcal{M} \pm \sigma_{\mathcal{M}}$	$d \pm \sigma_d$	$v \pm \sigma_v$	$t_0 \pm \sigma_{t_0}$
J0613-0200	19	0.01644 ± 0.004938	$-1.314 \times 10^{-15} \pm 4.172 \times 10^{-13}$	$-5.321 \times 10^{-10} \pm 3.357 \times 10^9$	53859 ± 0.0062922
J1024-0719	29	-0.4137 ± 0.07403	$1.186 \times 10^{-9} \pm 0.0538$	$2.584 \times 10^{-6} \pm 4.426 \times 10^{-6}$	55561 ± 3.185
J0034-0534	0	1.656 ± 0.3839	$-1.466 \times 10^{-8} \pm 654.6$	$1.236 \times 10^{-3} \pm 0.0004958$	52371 ± 23.047
J1024-0719	75	0.3192 ± 0.1049	$-2.109 \times 10^{-9} \pm 0.00826$	$2.841 \times 10^{-4} \pm 0.0004075$	56396 ± 6.8566
J1713+0747	211	0.03642 ± 0.009973	$-2.757 \times 10^{-8} \pm 0.00000118$	$2.035 \times 10^{-2} \pm 0.01307$	56271 ± 0.0002075
J1640+2224	3	0.06589 ± 0.01322	$-7.233 \times 10^{-9} \pm 0.00000815$	$4.909 \times 10^{-4} \pm 0.0008107$	53355 ± 0.0074092
J1857+0943	46	0.05748 ± 0.009663	$-9.726 \times 10^{-12} \pm 0.0001744$	$7.528 \times 10^{-9} \pm 2.009 \times 10^{-8}$	56120 ± 12.117
J1909-3744	175	0.01408 ± 0.003733	$1.534 \times 10^7 \pm 0.0004855$	$-2.204 \times 10^{-2} \pm 0.014$	56522 ± 0.022584
J1643-1224	17	0.4636 ± 0.09352	$-1.05 \times 10^6 \pm 7.695$	$5.348 \times 10^{-3} \pm 0.002258$	53994 ± 1.4459
J1024-0719	39	-0.2983 ± 0.07129	$-2.229 \times 10^{-12} \pm 7.177$	$1.422 \times 10^{-6} \pm 3.241 \times 10^{-6}$	55692 ± 2.2011
J0613-0200	72	0.03849 ± 0.01255	$1.936 \times 10^{-11} \pm 2.007 \times 10^{-10}$	$-1.55 \times 10^{-5} \pm 0.00005461$	55578 ± 0.00043247
J1643-1224	1	-2.206 ± 0.4336	$1.619 \times 10^{-6} \pm 15.02$	$6.51 \times 10^{-4} \pm 0.0002622$	51024 ± 17.367

Table 2. Summary of the fit parameters for the 12 events

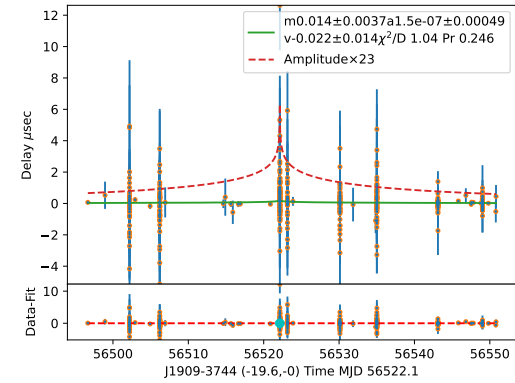
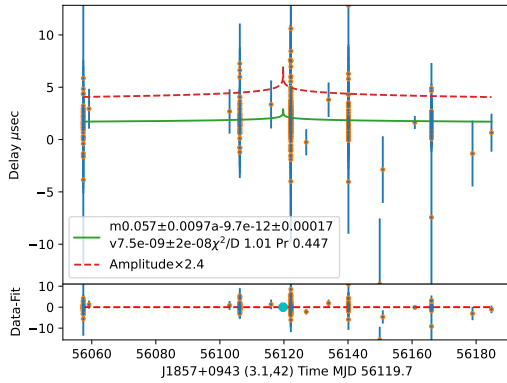
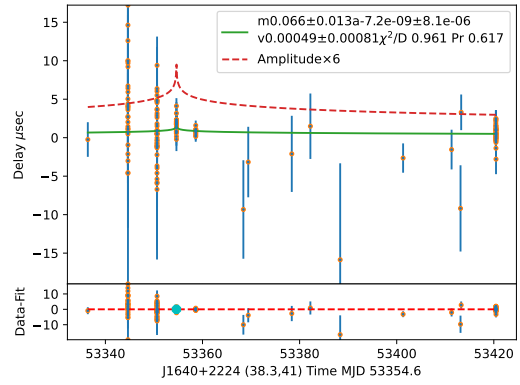
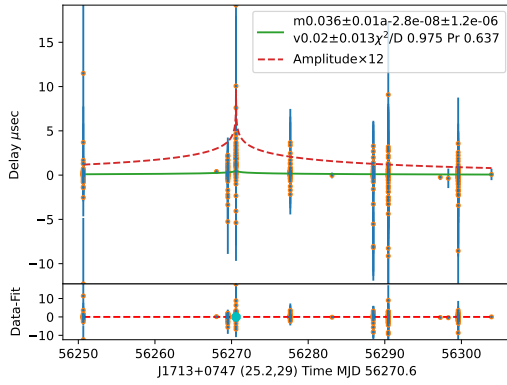
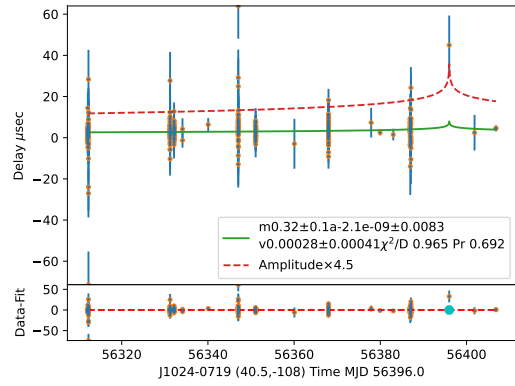
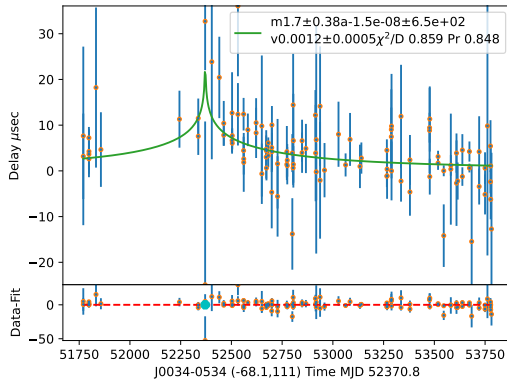
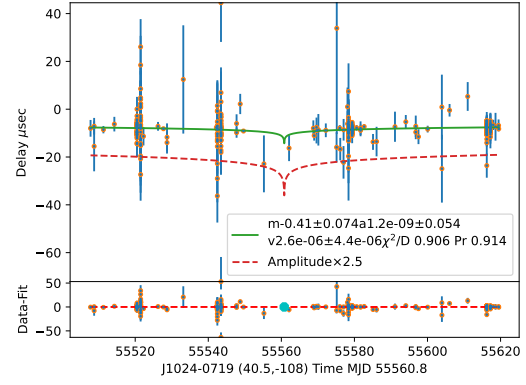
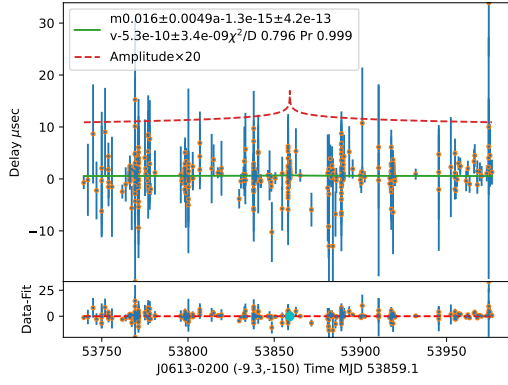
Table 1 lists the results of the search. The table includes details about the sample and results of the fit including the fitted mass and the χ^2/DOF probability. The number of residuals fit, the duration of the sample (in MJD) and the RMS of the sample in microseconds are also listed

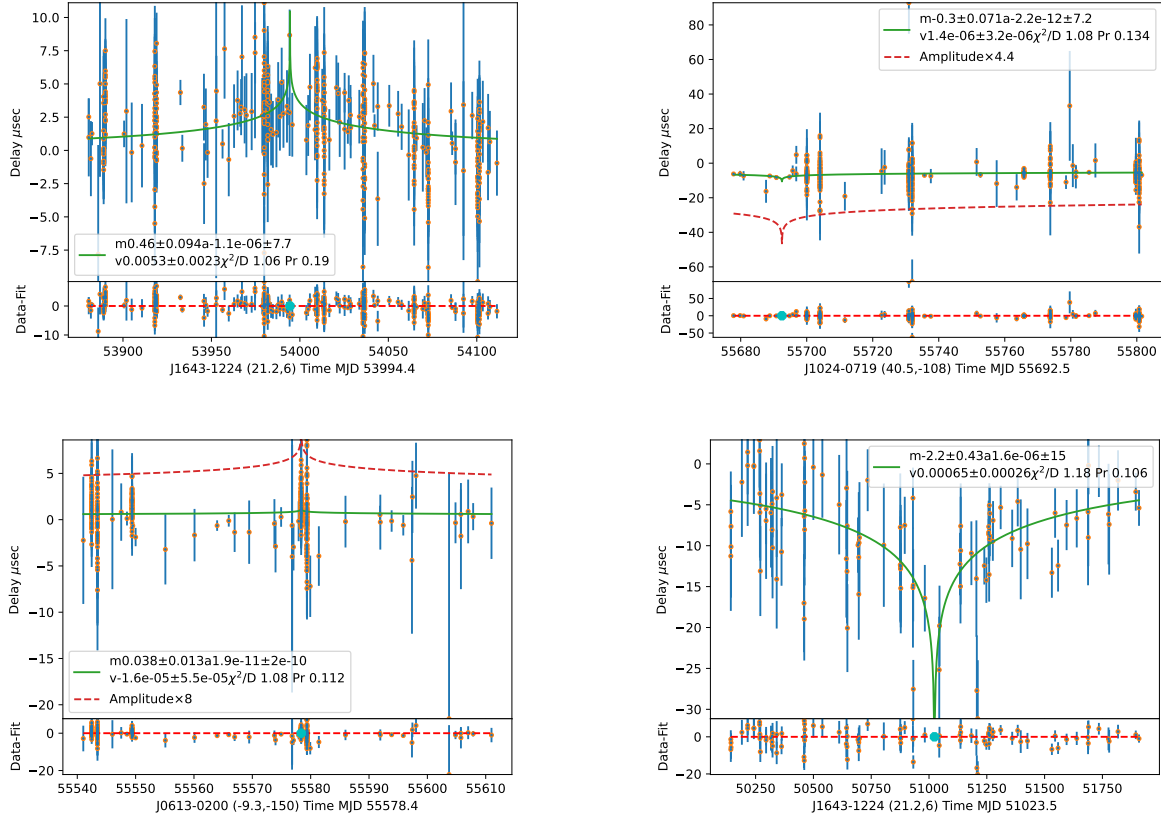
Table 2 includes the full list of the fitted parameters including d , v and the time of closest approach t_0 . There are no selection constraints on the values or significance of these parameters. These data are also printed on the plots.

7. FIGURES

Figures showing all the fits are displayed in this section. The figures are ordered from high to low by χ^2/DOF probability. Each figure has an upper panel showing the data and the fitted curve. The lower panel shows the data minus the fitted value of the delay curve, the new residuals. The dashed line on the lower curve is zero and the large point marks the position of the peak in the upper plot. The vertical axes on each plot are individually scaled and range from microseconds to tens of microseconds. The auto-scaling sometimes makes the signal peak hard to see due to large error bars on some of the points. The values for “vel”= v and “ang”= d printed on the plots are scaled by 10,000 to reduce the number of zeros to the right of the decimal.

If the fitted curve is small compared to the vertical scale of the plot a dashed red curve, a rescaled copy of the signal fit is also plotted. The legend gives the rescaling.





Pulsar	Sample Length (MJD)	Sample Size	Candidates
J0034-0534	4935.41	276	1
J0613-0200	5863.88	9322	2
J1024-0719	6647.34	5865	3
J1640+2224	6301.78	3097	1
J1643-1224	7356.24	8136	2
J1713+0747	8201.93	17487	1
J1857+0943	10344.48	5004	1
J1909-3744	3951.20	11483	1

Table 3. Summary of the data sample of the 8 pulsars

8. CONCLUSIONS

This article presents some evidence of detection of massive objects via their gravitational fields. There has been no attempt made to determine if the objects detected via timing delay are also visible via some other detection method. The measured masses may suggest a visible object. Since this paper has measured transients one may not be able to find a visible match in the same direction with data not collected at the same time. The fit yields an angular velocity on the sky but the direction in the plane is not known. This method does not provide a distance estimate for these objects except that it is limited by the distance to the pulsar source.

Three of the events in table 1 have $M < 0$ which is not compatible with the local mass hypothesis on which the fit function is based. These could be due to statistical fluctuations, noise, a systematic problem or something new. All three of these negative fits are found for pulsars, J1024-0719 and J1643-1224, that also have positive events in the table.

The cumulative distribution function of the χ^2 probability distribution is consistent with flat except for the region 0.1 to 0.2 which has 4 of the 12 events. This suggests that the sample has relatively little background except for the region 0.1 to 0.2 which shows some evidence for noise content.

One might expect noise events to be distributed uniformly in time or sample size. Table 3 lists exposure time and sample size for pulsars showing signals. The total data set spans 255327 MJD with 210148 timing residuals. The pulsar samples in table 3 represent 19% of the exposure time and 29 % of the timing residuals.

Some objects, such as rotating, Kerr-Newman, solutions have the potential to shorten travel times Pei (2021). But it is not clear if they would have the time profile fit for a relativistically induced time delay.

9. FUTURE POSSIBILITIES

Classic gravitational lensing Refsdal (1964) provides three observables, the time delay used in this analysis, amplification of the signal used in microlensing and multiple images. It may be possible to add these to the pulsar observables. The recorded energy may show changes correlated with the time delays or one may be able to discern changes in the apparent source size correlated with the delay. Even modest additional input may help reject noise events and better characterize true lensing sources.

ACKNOWLEDGMENTS

This work would not have been possible without the efforts of the maintainers of the PPTA second data release and the Tempo2 code used to fit the residuals. Jim Rich has been an invaluable aid in understanding the microlensing method of observing dark matter that has many concepts in common with those used here.

REFERENCES

- T.I Larchenkova and O.V. Doroshenko, “Pulsars as a Tool for Detection of Dark Matter in the Galaxy” *Astron. Astrophys.* **297**, 607-609 (1995)
- L. Wyrzykowski *et al.*, “Gaia Data Release 3 Microlensing Events from All Over the Sky” *Astron. Astrophys.* **abc**, 1-45 (2022). (arXiv:2206.06121)
- Irwin I. Shapiro (1964), “Fourth Test of General Relativity”, *Phys. Rev. Lett.* **13** (26): 789–791 (1964).
- S. Weinberg, “Gravitation and Cosmology”, Wiley & Sons, New York, (1972).
- T.I Larchenkova and A.A. Lutovinov (2007), “On the Possibility of Observing the Shapiro Effect for Pulsars in Globular Clusters”, *Astro. Lett.* **33** (7): 455-467 (2007)
- S. Desai and E.O. Kahya (2016), “Galactic one-way Shapiro delay to PSR B1937+21”, *Mod. Phys. Lett. A* **31** (13): 1650083-1 - 1650083-14 (2016).
- M. Kerr *et al.*, “The Parkes Pulsar Timing Array project: second data release”, *Publications of the Astronomical Society of Australia*, **37**, e020 (2020)
- D.J. Reardon *et al.*, “The Parkes pulsar timing array second data release: Timing analysis”. *MNRAS*, **507**, 2137-2153 (2021).
- J. Antoniadis *et al.*, “The International Pulsar Timing Array second data release: Search for an isotropic Gravitational Wave Background”, *MNRAS*, **510** 4873-4887 (2022).
- R.T. Edwards, G.B. Hobbs, R.N. Manchester, “tempo2, a new pulsar timing package – II. The timing model and precision estimates”, *MNRAS*, **372**, 1549-1574 (2006).
- Irwin I. Shapiro *et al.*, “Fourth Test of General Relativity: Preliminary Results”, *Phys. Rev. Lett.* **20**, 1265–1269 (1968).
- Ting-Hang Pei, “The Superluminal Phenomenon of Light Near the Kerr–Newman Black Hole or Super-Gravitational Source”, *Front. Phys.*, Volume 9 - 2021 | <https://doi.org/10.3389/fphy.2021.701619> (2021).
- Tien Hsieh, Da-Shin Lee and Chi-Yong Lin. “Gravitational time delay effects by Kerr and Kerr-Newman black holes in strong field limits”, *Phys. Rev D* **104**. 104013 (2021).
- Sjur Refsdal, “The Gravitational Lens Effect”, *MNRAS*, **128** 295-306 (1964).